LANGMUIR

pubs.acs.org/Langmuir Article

Dynamic Surfaces—Degradable Polyester Networks that Resist Protein Adsorption

Gaoyan Mu, C. K. Pandiyarajan, Xiuyuan Lu, Matt Weaver, Jan Genzer, and Christopher B. Gorman*

Cite This: *Langmuir* 2021, 37, 8978–8988 Read Online

ACCESS | Metrics & More | Article Recommendations | Supporting Information

ABSTRACT: We synthesized a series of novel degradable alternating copolyesters composed of diglycolic anhydride (DGA) and two epoxides, epoxymethoxytriethylene glycol (ETEG) and a photoactive crosslinking agent epoxy benzophenone (EBP). After UV crosslinking, soaking the films in a good solvent (tetrahydrofuran) removed uncrosslinked material, and the resulting film gel fractions were calculated. These network films were then degraded in buffer solutions of varying pH values. The degradation of networks with lower gel fraction (fewer crosslinks) was faster and followed first-order kinetics. In contrast, the denser network degraded slower and followed zeroth-order kinetics. The lower gel fraction networks possess a higher swelling ratio and resist bovine serum albumin (BSA) adsorption better by entropic shielding and faster degradation. In comparison, higher gel fraction networks with higher EBP mole fractions adsorb more BSA due to hydrophobic interactions and slower degradation.

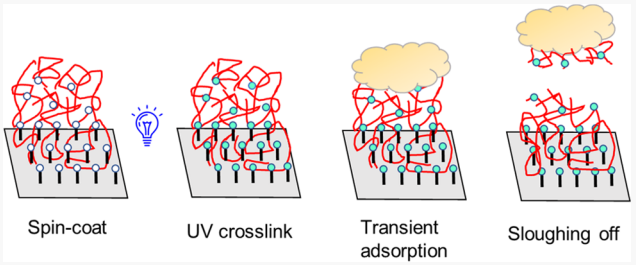

Downloaded via NORTH CAROLINA STATE UNIV on August 3, 2021 at 17:59:21 (UTC).
See https://pubs.acs.org/sharingguidelines for options on how to legitimately share published articles.

INTRODUCTION

Biofouling of surfaces is a global problem. Biomass accumulation on ship hulls generates high frictional resistance, increasing fuel consumption, and overall travel costs up to 77%.[1] Moreover, it is reported that about 26% of health-care-related infections are caused by device-associated infections and more than 45% of hospital-relevant infections can be traced to biofilm-infected medical devices.[2] Biofouling therefore results in large economic losses and threatens lives. The first step in biofouling is the adsorption of proteins to a surface.[3] Thus, there has been considerable effort to prepare surfaces that resist the adsorption of proteins. Various antibiofouling coatings, including poly(ethylene glycol) (PEG)-based coatings,[4] fouling release coatings,[5] zwitterionic polymers,[6] and amphiphilic polymers[7] have been synthesized and studied. Many of these retard the adsorption of proteins, but most do not do so for a long period (greater than a few hours). Thus, it is of interest to explore strategies that avoid biofouling over longer periods of time.

Here, we report new, dynamic, biodegradable coatings on surfaces and study whether they improve the lifetime of surfaces against biofouling. Biodegradable polyester[8] and other[9] brushes have shown some promise in this regard,[8] but they are thin (ca. 10 nm) and degrade off of the surface relatively quickly. Here, we report the formation of ca. 60 nm thick, surface-anchored, crosslinked polyester films formed by spin-coating and UV irradiation as a new type of dynamic surface to prevent protein adsorption. The crosslink density was controllable by altering the mole fraction of the crosslinker in the polymer. These films are thicker than polymer brushes generated by surface-initiated polymerization, and their preparation process is more convenient and reproducible.[10] It will be shown that these films resist bovine serum albumin (BSA) adsorption well for up to 38 h.

EXPERIMENTAL SECTION

Materials. Diglycolic anhydride (DGA), epichlorohydrin, potassium dihydrogen phosphate, potassium phosphate dibasic, sodium hydride, sodium hydroxide, hydrochloride acid, 4-hydroxyl benzophenone, allyl bromide, potassium carbonate, triethoxysilane, platinum/carbon, magnesium sulfate, chromium salen, bis(triphenylphosphine) iminium chloride ([PPN]Cl), 0.8 M phosphazene base P_4-*t*-Bu solution in hexane, sodium phenylmethanolate, bovine serum albumin (BSA), albumin–fluorescein isothiocyanate conjugate (fluorescent BSA) were purchased from Sigma-Aldrich (St. Louis, MO). All solvents were obtained from VWR (Atlanta, GA). Silicon wafers were purchased from ePAK International Inc (Austin, TX).

Instrumentation. All monomers and polymers were characterized by proton nuclear magnetic resonance (^{1}H NMR, 400 MHz) spectroscopy and carbon-13 nuclear magnetic resonance (^{13}C NMR, 100 MHz) spectroscopy (Varian USA or Bruker USA). The silicon wafers were cleaned using a UVO-cleaner (Model No. 42, Jelight Company, Inc., 2 Mason, Irvine, CA). The polymer films were deposited by a spin coater (PNM32 model, Headway Research, Inc.). The molecular weights of polymers were determined by size exclusion

Received: March 31, 2021
Revised: July 9, 2021
Published: July 23, 2021

ACS Publications © 2021 American Chemical Society

https://doi.org/10.1021/acs.langmuir.1c00890
Langmuir 2021, 37, 8978–8988

Scheme 1. Ring-Opening Polymerization of Diglycolic Anhydride and Two Epoxides

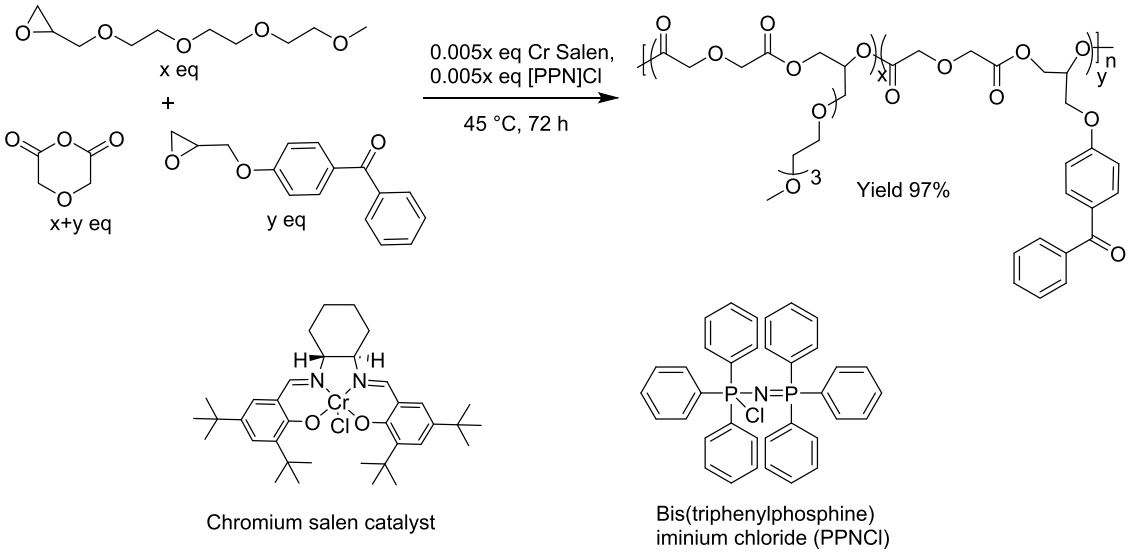

chromatography (SEC)—Shimadzu2.0. (Shimadzu Corporation, Columbia, MD). The thickness of thin films was measured by variable-angle spectroscopic ellipsometry (VASE, J.A. Woollam). An Omnicure series-1000 UV lamp activated the photoactive crosslinking reactions at a wavelength of 365 nm (Lumen Dynamics). The UV light intensity was examined by an ILT1400-A radiometer/photometer (International Light Technology). The coatings containing fluorescent BSA were observed under Olympus BX61 fluorescence microscope (Olympus). The morphology of surfaces was investigated via atomic force microscopy (AFM) using an Asylum MFP-3D classic atomic force microscope (Oxford Instruments). The water contact angles were measured using a Rame Hart contact angle goniometer. The surface functionality was characterized by Fourier transform-infrared spectroscopy (FT-IR) in attenuated total internal reflectance (ATR) mode (Nicolet 6700 by Thermo Scientific).

Synthesis of Epoxymethoxytriethylene Glycol (ETEG). A two-necked round-bottomed flask was loaded with 6.92 g of sodium hydride (60% in oil) and purged with nitrogen. The flask was filled with 50 mL of hexanes via syringe and stirred. The sodium hydride was allowed to settle, and the hexanes were removed via syringe. This washing process was repeated three times. After the last hexane wash, 30 mL of tetrahydrofuran (THF) was added to the flask. The flask was placed in an ice bath, and 25 mL of triethylene glycol monomethylether was slowly added via a pressure-equalizing addition funnel. The reaction was allowed to react for 2 h at room temperature in a water bath. The flask was placed in an ice bath, and 25 mL of epichlorohydrin was slowly added via a pressure-equalizing addition funnel. The reaction was allowed to react for 16 h at room temperature and refluxed for 4 h (see Scheme S1). Upon completion, the raw product was centrifuged. The salt was washed two times with tetrahydrofuran (THF), and the THF was combined with the organic solution. The solvents were removed via rotatory evaporation. The final product was distilled under vacuum to give 25 g of a transparent liquid (76% yield). ^{1}H NMR (400 MHz; $CDCl_3$): δ 7.26 (s, $CDCl_3$), 3.76 (dd, 1H), 3.64 (br, 10H), 3.53 (m, 2H), 3.40 (dd, 1H), 3.36 (s, 3H), 3.14 (m, 1H), 2.77 (m, 1H), and 2.58 (m, 1H). ^{13}C NMR (100 MHz; $CDCl_3$): δ 77.16 ($CDCl_3$), 71.9, 71.9, 70.7, 70.5, 59.0, 50.8, and 44.2.

Synthesis of Epoxybenzophenone (EBP). Three grams (15 mmol) of 4-hydroxybenzophenone was dissolved in 25 mL (320 mmol) of epichlorohydrin in a 100 mL round-bottom flask, and 1.0 g (25 mmol) of sodium hydroxide beads were added. The reaction was refluxed for 5 h at 130 °C (see Scheme S2). The raw product was filtered, and the solid residue was washed with diethyl ether. The organic phases were combined and washed with water three times and dried with anhydrous magnesium sulfate. The solvent was removed by rotatory evaporation and a solid white product (2.5 g) was obtained (65% yield). ^{1}H NMR (400 MHz; $CDCl_3$): δ 7.80 (m, 4H), 7.47 (m, 3H), 7.26 (s, $CDCl_3$), 7.00 (m, 2H), 4.32 (m, 1H), 4.04 (m, 1H), 3.40 (m, 1H), 2.95 (m, 1H), and 2.79 (m, 1H). ^{13}C NMR (100 MHz; $CDCl_3$): δ 195.5, 162.0, 138.2, 132.6, 132.0, 130.7, 129.8, 128.2, 114.2, 77.16 ($CDCl_3$), 68.9, 49.9, and 44.6.

Alternating Copolymerization of Diglycolic Anhydride and Two Epoxides. DGA and EBP were dried by azeotropic distillation with dry benzene and stored in a glovebox. Toluene was distilled and stored in a glovebox. ETEG was distilled and stored over molecular sieves in a glovebox. A 4 mL vial equipped with a stir bar was flame-dried and immediately transferred into the glovebox. Then, 0.23 g (2.0 mmol) of DGA, 0.051 g (0.20 mmol) of EBP, 0.37 mL (0.18 mmol) of ETEG, 0.006 g (0.01 mmol) of chromium salen, and 0.005 g (0.01 mmol) of [PPN]Cl were dissolved in 0.3 mL of toluene in this vial. The solution was stirred for 3 days at 45 °C in the glovebox (see Scheme 1). Upon completion, the solvent was removed by rotatory evaporation. A few drops of dichloromethane (DCM) were added, and the solution was precipitated in 20 mL of diethyl ether. The polymer was collected after centrifugation and dried under a high vacuum overnight. The example described here is the polymer with 5 mol % EBP. For all samples, the product was a viscous, off-yellow liquid (97% yield). ^{1}H NMR (400 MHz; $CDCl_3$): δ 7.79 (m, 4H), 7.59 (m, 3H), 7.26 (s, $CDCl_3$), 6.98 (m, 2H), 5.28 (m, 1H), 4.47 (m, 1H), 4.25 (s, 5H), 3.62 (br, 14H), and 3.38 (s, 3H). ^{13}C NMR (100 MHz; $CDCl_3$): δ 169.5, 138.0, 132.6, 132.1, 129.8, 128.3, 114.1, 77.16 ($CDCl_3$), 72.3, 71.9, 70.9, 70.6, 70.4, 69.1, 68.4, 68.3, 67.9, 67.8, 66.0, 63.1, 59.0, and 53.4.

Synthesis of Polyether. ETEG and EBP were purified by the same method described in the Synthesis of Epoxymethoxytriethylene Glycol (ETEG) section. A 4 mL vial equipped with a stir bar was flame-dried and immediately transferred into a glovebox. In the glovebox, 220 μL (0.96 mmol) of ETEG, 30 mg (0.11 mmol) EBP, 1.3 mg (0.010 mmol) sodium phenylmethanolate, 80 μL (0.064 mmol) of phosphazene base P4-t-Bu solution, and 80 μL of toluene were mixed and stirred for 3 days at room temperature (see Scheme S3). Upon completion, the solvent was removed by rotatory evaporation. The polymer was precipitated in cold hexane to obtain a clear, viscous liquid (90% yield). ^{1}H NMR (400 MHz; $CDCl_3$): δ 7.79 (m, 4H), 7.59 (m, 3H), 7.26 (s, $CDCl_3$), 6.98 (m, 2H), 3.73 (br, 15H), 3.48 (s, 3H), and 2.65 (d, 2H). ^{13}C NMR (100 MHz; $CDCl_3$): δ 132.5, 129.6, 128.2, 114.2, 78.8, 77.16 ($CDCl_3$), 72.5, 71.9, 71.3, 70.8, 70.6, 70.5, 69.6, 67.1, 59.0, and 37.3.

Preparation of Polymer Anchored on the Silicon Substrate. 4-[3-(Triethoxysilyl)propyloxy]-benzophenone (TESPBP) was synthesized following the procedure provided in the literature, as shown

https://doi.org/10.1021/acs.langmuir.1c00890
Langmuir 2021, 37, 8978−8988

in Scheme S4.[11] Thirty millimoles of freshly prepared TESPBP were dissolved in toluene and spin-coated onto the UVO-cleaned silicon wafer (1500 rpm, 45 s spinning). Next, the sample was annealed in the oven overnight at 110 °C, followed by extraction in toluene and drying under N_2 gas. A functionalized silicon wafer coated with 2−3 nm of TESPBP was obtained. Polyester samples were dissolved in dry dioxane and filtered through a 0.2 μm poly(tetrafluoroethylene) (PTFE) membrane to prepare 20 mg/mL stock solution. The polymer solutions were then spin-coated onto the TESPBP-functionalized silicon wafer (2500 rpm, 30 s spinning). The prepared layer was illuminated with UV light at 365 nm with a dosage of 30 mW/cm^2 for 5 min. The specimen was then extracted with THF overnight to remove any uncrosslinked polymer from the substrate leaving the crosslinked polyester network attached to the substrate (50−75 nm).

Allyloxy Benzophenone. ^{1}H NMR (400 MHz; $CDCl_3$): δ 7.79 (m, 4H), 7.59 (m, 3H), 7.26 (s, $CDCl_3$), 6.07 (m, 1H), 5.37 (m, 2H), and 4.63 (d, 2H). ^{13}C NMR (100 MHz; $CDCl_3$): δ 195.5, 162.2, 138.3, 132.5, 131.9, 130.3, 130.0, 129.7, 128.4, 128.2, 118.2, 114.3, 77.16 ($CDCl_3$), and 68.9.

TESPBP. ^{1}H NMR (400 MHz; $CDCl_3$): δ 7.79 (m, 4H), 7.59 (m, 3H), 7.26 (s, $CDCl_3$), 6.07 (m, 1H), 4.02 (t, 2H), 3.78 (q, 6H), 1.93 (m, 2H), 1.23 (t, 9H), and 0.78 (t, 2H). ^{13}C NMR (100 MHz; $CDCl_3$): δ 195.5, 162.2, 138.3, 132.5, 131.8, 129.9, 129.7, 128.2, 114.0, 77.16 ($CDCl_3$), 70.1, 59.2, 58.5, 58.4, 22.7, 18.1, and 6.5.

Preparation of Polymer Anchored on the Gold Substrate. To acquire good FT-IR signals of spin-coated films, gold substrates were utilized. To covalently anchor a polyester film on gold, the gold surface was functionalized by benzophenone disulfide. This molecule was synthesized as follows. A 100 mL Schlenk flask was charged with allyloxy benzophenone (600 mg, 2.52 mmol, 1 equiv), AIBN (0.30 mmol, 50 mg, 0.12 equiv), MeCOSH (6.30 mmol, 450 μL, 2.5 equiv), and anhydrous THF (10 mL). The resulting solution was degassed three times with N_2. The mixture was stirred and maintained at 60 °C for 3 days (see Scheme S5). The mixture was then concentrated and purified by mobile phase liquid chromatography (DCM/hexane = 2:1) to give 800 mg of S-(3-(4-benzoylphenoxy)propyl) ethanethioate (yield: 76%). ^{1}H NMR (400 MHz; $CDCl_3$): δ 7.78 (m, 4H), 7.55 (t, 1H), 7.60 (t, 2H), 6.94 (d, 2H), 7.26 (s, $CDCl_3$), 4.08 (t, 2H), 3.06 (t, 2H), 2.34 (s, 3H), and 2.09 (m, 2H). ^{13}C NMR (100 MHz; $CDCl_3$): δ 195.9, 162.4, 138.3, 132.6, 131.9, 130.2, 129.8, 128.2, 114.1, 77.1 ($CDCl_3$), 66.4, 30.7, 29.3, and 26.0.

To a solution of S-(3-(4-benzoylphenoxy)propyl) ethanethioate (800 mg, 2.54 mmol, 1 equiv) in MeOH−THF (26 mL, 1:1) was added powdered lithium hydroxide (6.26 mmol, 150 mg, 2.46 equiv). The mixture was stirred 24 h open to air, and concentrated HCl (1 mL) was then added. The mixture was concentrated and extracted with DCM (three times). The organic phases were combined, dried with anhydrous magnesium sulfate, and concentrated (see Scheme S6). Column chromatography (DCM/hexane = 2:1) gave 400 mg of product (yield: 58%). ^{1}H NMR (400 MHz; $CDCl_3$): δ 7.78 (m, 8H), 7.55 (t, 2H), 7.60 (t, 4H), 6.94 (d, 4H), 7.26 (s, $CDCl_3$), 4.09 (t, 4H), 2.85 (t, 4H), and 2.17 (m, 4H). ^{13}C NMR (100 MHz; $CDCl_3$): δ 195.5, 162.4, 138.3, 132.6, 131.9, 130.2, 129.7, 128.2, 114.0, 77.1 ($CDCl_3$), 66.4, 34.9, and 28.6.

Self-assembled monolayers (SAMs) of dibenzophenone disulfides were prepared by immersing cleaned gold surfaces in 1 mM dibenzophenone disulfide solution of DCM for 3 days. Then, the polyester was spin-coated on gold surfaces analogous to what was performed on silicon/silica previously.

Determination of Gel Fraction. Gel fraction (P_{gel}) was calculated according to eq 1. We used VASE to measure the film thickness of the deposited layers. After spin-coating and crosslinking, the initial film thickness h_0 was measured. The film was extracted in THF overnight, dried with N_2, and the layer thickness h_t was measured to determine the value of P_{gel}.

$$P_{gel} = \frac{h_t}{h_0} \tag{1}$$

Degradation of Network Films. The degradation of the polyester network was investigated based on the thickness change of samples immersed in phosphate-buffered saline (PBS) solution with various pH values. The PBS solution was prepared by potassium dihydrogen phosphate and potassium phosphate dibasic with 1 M ionic strength. The pH values were adjusted to 6.4, 7.0, 7.4, 8.2 via hydrochloric acid and sodium hydroxide. Only small amounts of acid or base were required, so the change in ionic strength was minimal. Wafers were immersed in PBS solutions in 20 mL vials and placed on the shaker at 200 rpm. Wafers were taken out of the buffer solution at specific time points, washed by DI water, dried with N_2 gas, and the film thickness was measured via VASE.

Protein Adsorption. Protein solutions with different concentrations (1 and 3 mg/mL) were prepared by dissolving albumin−fluorescein isothiocyanate conjugate protein or BSA in PBS solution. The polyester network coatings were immersed in these solutions in 20 mL vials and placed on a shaker table at 150 rpm. The specimens were taken out at specific time intervals, washed with DI water, and dried with N_2. Any change in film thickness was measured via VASE, and the specimen was observed under a fluorescence microscope. The albumin−fluorescein isothiocyanate conjugate protein has 7−12 moles of fluorescein isothiocyanate (FITC) per mole of albumin. The excitation and emission wavelength for FITC are 495 and 519 nm, respectively. Integrated fluorescence intensity over a 100 μm × 100 μm region was obtained using ImageJ.[12]

Contact Angle Measurements. Wettability of the surface-attached networks was characterized by contact angle measurements using Ramé−Hart contact angle goniometer (model no. 100-00, Succasunna, NJ) equipped with a liquid dispenser, camera, and image-processing software. A drop of DI water with a volume of ∼5 μL was placed on the wafer, and static contact angles were measured. The average contact angle was determined over 3−5 measurements.

Swelling of Network Films. The swollen thickness of the film was measured by an ellipsometer equipped with a liquid cell. The cell was filled with ca. 100 mL of DI water. The specimen was immersed in DI water for 1 min to reach equilibrium. The reflectivity scans were recorded at a 70° angle of incidence in the 400−1000 nm spectral range in 60 steps (10 nm/step).[11]

Preparation of Bulk Gel. A polyester with 7.5% EBP feed ratio was dissolved in THF to make a 200 mg/mL polymer solution. The solution was then drop-coated on a glass slide. The slide was placed in a vacuum oven at 60 °C for 3 h. The specimen was then irradiated under 370 nm UV light with a dosage of 40 mW/cm^2 for 2 h to make the gel. Then, the gel was extracted in THF to remove any unreacted materials that are not part of the gel and dried under vacuum.

Swelling of Bulk Gels. The gel was transferred into a small, tared vial and weighed with an accuracy of 0.1 mg. The gel was immersed in DCM for 2 h to reach equilibrium. The solvent was removed by micro-pipette, and the total weight of the vial and the swollen gel was recorded until the weight variation was <0.5%. The swelling ratio of bulk gels was calculated as shown in eq 2.

$$\alpha_{3D}^{bulk} = \left(\frac{V_{polymer} + V_{solvent}}{V_{polymer}}\right) = \left(1 + \frac{m_{solvent}}{m_{polymer}}\frac{\rho_{polymer}}{\rho_{solvent}}\right) \tag{2}$$

In eq 2, $m_{solvent}$ and $m_{polymer}$ represent the masses of the solvent and the polymer, respectively, and $\rho_{polymer}$ (1.18 g/mL) and $\rho_{solvent}$ (1.33 g/mL) indicate the densities of the polymer and solvent, respectively.[11] The calculated swelling ratio of 5 mol % EBP gel in DCM is 5.20.

RESULTS AND DISCUSSION

The synthesized polyester has a hydrophilic and hydrolyzable backbone. The epoxymethoxytriethylene glycol (ETEG) was chosen as one of the epoxide sources to improve the hydrophilicity of the side chain. Triethylene glycol groups are also known to resist protein adsorption.[4,13,14] Another epoxide (epoxy benzophenone (EBP)) was employed as a UV-active crosslinker that forms networks upon UV irradiation.

https://doi.org/10.1021/acs.langmuir.1c00890
Langmuir 2021, 37, 8978−8988

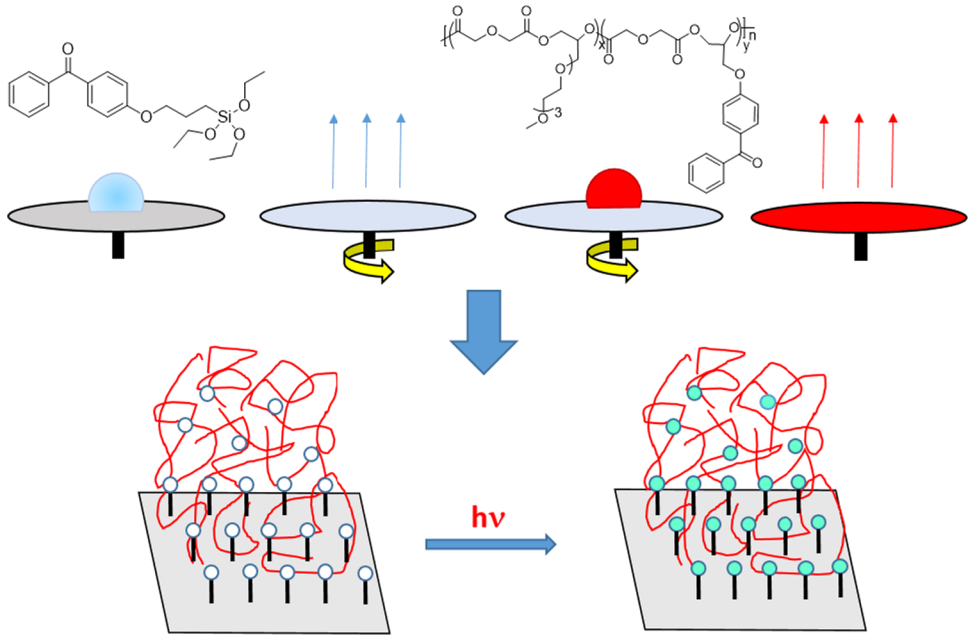

Figure 1. Cartoon illustrating the formation of crosslinked films anchored covalently to the surface via the BP groups.

The incorporation of diglycolic anhydride is hypothesized to impart functionality similar to that of poly(ethylene glycol) yet further incorporates a biodegradable ester linkage. The chromium salen is a Lewis acid catalyst reported by Coates et al.[15] [PPN]Cl was used as a co-catalyst, introducing chloride ions to initiate polymerization and PPN^+ as a noncoordinating cation.

Alternating copolyesters with different mole fractions of EBP in the feed ratio were synthesized by a perfectly alternating ring-opening polymerization of a 200:200:1:1 molar feed ratio of anhydride to (total) epoxide to Cr salen catalyst to co-catalyst at 45 °C (Table S1).[16] The perfectly alternating copolymerization was confirmed by ^{13}C NMR, which showed no ether linkages in the backbone appearing at 78 ppm (Figure S6). These would be present if there were two sequential ring openings and additions of epoxide, which were not observed. The EBP mole fraction in Table S1 was determined by ^1H NMR integration as described in Supporting Information (Figure S5). Number-average molecular weights and molecular weight dispersity ($Đ$) of polymers were measured by SEC, with polystyrene standards as a reference. The degree of polymerization (one epoxide plus one anhydride was regarded as one repeat unit) was calculated. The value of X_{avg} represents the calculated average number of crosslinked units (EBP) per 100 polymer chains. These polymers are of relatively low molecular weight and higher polydispersity compared to other copolyesters reported in the literature.[15a17] However, they were able to be spin-coated into thin films (see below) and thus served their purpose.

Surface-Attached Networks. After synthesizing precursor copolymers, the copolymers were anchored on the substrate and crosslinked. Benzophenone (BP) can act as a photoactive crosslinker.[18] Under the irradiation of UV light, BP units form triplet $C^{\bullet}-O^{\bullet}$ biradicals. Those radicals will promiscuously abstract hydrogen atoms from adjacent groups, creating two radicals that recombine to form a covalent bond. A BP-terminated triethoxysilane was spin-coated from toluene solutions onto thin silica layers on silicon wafers to prepare BP-functionalized silicon wafers. Solutions of BP-containing ter-polyesters were then spin-coated onto these wafers as described in the Experimental Section. These samples were irradiated to simultaneously crosslink the films and covalently anchor them to the substrate (Figure 1). The benzophenone adlayer acts as surface anchors and suppresses delamination of the polymer film from the substrate after UV irradiation.[19] After measuring their thicknesses, the specimens were incubated in tetrahydrofuran (THF) for 18 h, removed, dried, and their thicknesses were again measured to determine their gel fraction (Table S1). As the irradiation time increased, the gel fraction increased until a plateau was reached (Figure S13). All samples were irradiated under 30 mW/cm^2 UV light for 5 min to maximize the crosslink density. It was then verified that no further changes in gel fraction occurred due to further irradiation with ambient light.

As expected, the EBP/ETEG ratio affected the final gel fraction of the sample. Specifically, X_{avg} values correlated with the EBP ratio in the monomer feed. Likewise, the gel fraction correlated with EBP ratio and X_{avg}, with larger gel fractions found for samples with larger X_{avg} values for most cases. We prepared samples with gel fractions ranging from ∼0.4 to ∼0.9.

Degradation of Networks. The hydrolytic degradation of polyesters has been studied in detail. These studies include the effects of pH and gel fraction on the rate and mechanism of degradation.[20] The effects of crosslinking and solvent composition on the degradation of polyesters have been studied previously in bulk, but not in thin films.[21b−d,22] Network films with different gel fractions were immersed in PBS solutions at various pH values, taken out, and their thickness was measured by VASE.

Figure 2 shows the percent change in thickness of the gel over time for three different gel fractions (results from other samples/gel fractions are shown in Figure S14). The percentage change in thickness was calculated from h_t/h_0, where h_t represents thickness at each specific time and h_0 is the initial thickness before extraction with THF. The data in Figure 2 indicate that the degradation rate of the networks increases with increasing pH. The most likely mechanism of degradation of the networks involves ester hydrolysis. This

https://doi.org/10.1021/acs.langmuir.1c00890
Langmuir 2021, 37, 8978−8988

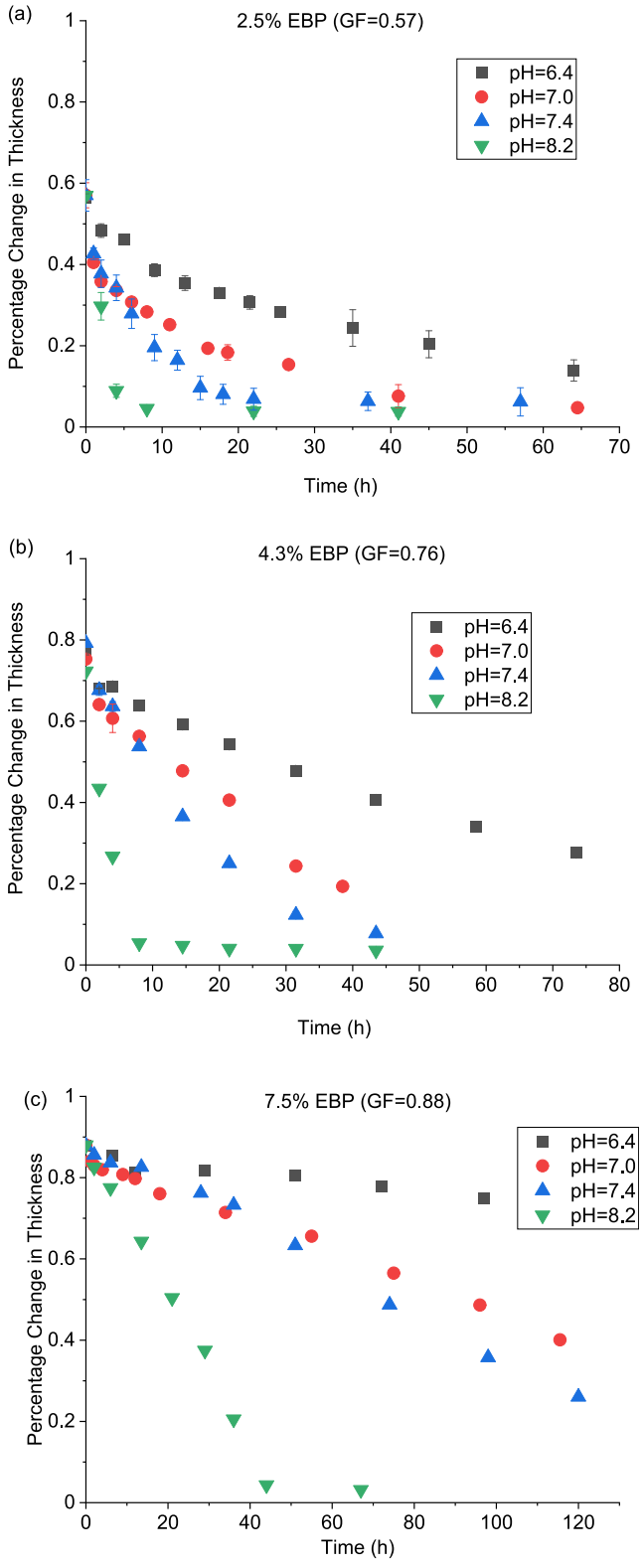

Figure 2. Percentage change of thickness of samples with different gel fractions (GF = 0.57, 0.76, 0.88) in PBS buffer solution (ionic strength = 1 M) with various pH values. In (a), each data point is the average value of three measurements on different films. In (b, c), each data point is the average value of three measurements on different locations of the film. The error bars are smaller than the size of the plot symbols used. The variability in the gel fraction of the samples in each plot is in the range of ±1 to ±5%.

hydrolysis is both acid- and base-catalyzed, but base-catalyzed hydrolysis is faster.[23] To support this mechanism, 40 mg of polymer (5% EBP) was dissolved in 0.8 mL of THF, mixed with 2.6 mL 0.10 M KOH methanol solution, and shaken for 1 day. After the completion, the residue was analyzed by ^{1}H and ^{13}C NMR (Figures S15 and S16). The signals of methylene groups adjacent to ester groups at 4.25 and 4.48 ppm (^{1}H NMR), 69.21 and 67.92 ppm (^{13}C NMR) disappeared. The ester hydrolysis can also be catalyzed by acid but requires a lower pH than the range examined in Figure 2. Immersing the films in more acidic solutions (pH from 1 to 3) resulted in faster degradation than at pH 6.4 (Figure S17). The degradation mechanism of the thin film in buffer solution was also studied by ATR−FTIR spectroscopy. The polymer was spin-coated on a gold surface, crosslinked by UV irradiation, and then immersed in pH 7.4 buffer solution overnight. Surface functional groups of the thin film before and after degradation were analyzed by ATR−FTIR, as shown in Figure S18. After degradation, the carbon−oxygen single-bond signal at 1240 cm^{-1} decreased, and that of the hydroxyl at 3300 cm^{-1} increased. From these data, we conclude that the degradation of the network is via ester hydrolysis.

The data in Figure 2 also indicates that degradation is faster in networks with lower gel fractions. Examining these data more closely, at lower gel fraction, the rate of the decrease of film thickness was exponential. In contrast, at higher gel fractions, the rate of the decrease of film thickness was close to linear. These behaviors suggest a change in the kinetics of degradation as gel fraction varies from low to high. The exponential decrease is a hallmark of first-order kinetics, while a linear decrease is a hallmark of zeroth-order kinetics. For example, the network with a 0.57 gel fraction (Figure 2a) displays first-order degradation kinetics.

$$\frac{-\mathrm{d}h}{\mathrm{d}t} = k_1 \cdot h \tag{3}$$

which, integrated, gives

$$h_t = h_0 \cdot e^{-k_1 t} \tag{4}$$

In eqs 3 and 4, h_0 is the thickness at time zero, h_t is the thickness at time t, and k_1 is the rate constant. On the other hand, there is a linear decrease in thickness with increasing time for a higher gel fraction (0.88) sample (Figure 2c), which follows the zeroth-order degradation kinetics (see eqs 5 and 6). The degradation rate is independent of the thickness of the film.

$$\frac{-\mathrm{d}h}{\mathrm{d}t} = k_0 \tag{5}$$

which, integrated, gives

$$h_t = h_0 - k_0 t \tag{6}$$

Figure 3a plots the apparent first-order rate constant (k_1) for low gel fraction samples, and Figure 3b plots the apparent zeroth-order rate constant (k_0) for high gel fraction samples. In both cases, the rate constant decreases with decreasing pH. The first-order rate constant appears to be independent of the gel fraction at a given pH. The zeroth-order rate constants decrease with increasing gel fraction. A rationale for this behavior is given below.

There are two possible ways to explain why films with lower gel fractions degrade faster. The first one is that there is a

https://doi.org/10.1021/acs.langmuir.1c00890
Langmuir 2021, 37, 8978−8988

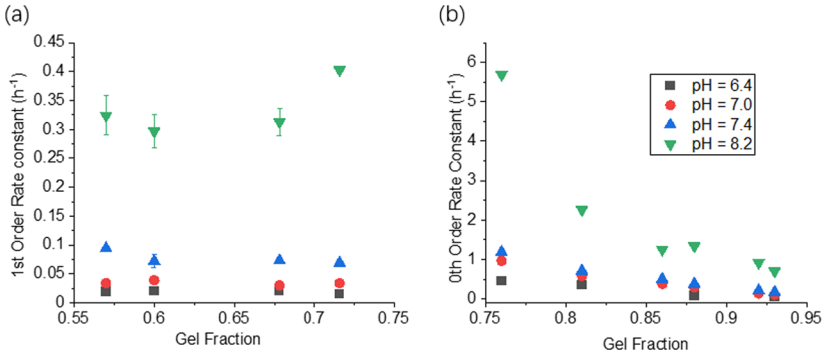

Figure 3. (a) Plot of first-order rate constant versus gel fraction in the low gel fraction range and (b) plot of zeroth-order rate constant versus gel fraction in the high gel fraction range in PBS buffer solution with different pH values. Each data point is the average value of three measurements on different locations of the film. Some error bars are smaller than the size of the plot symbols used.

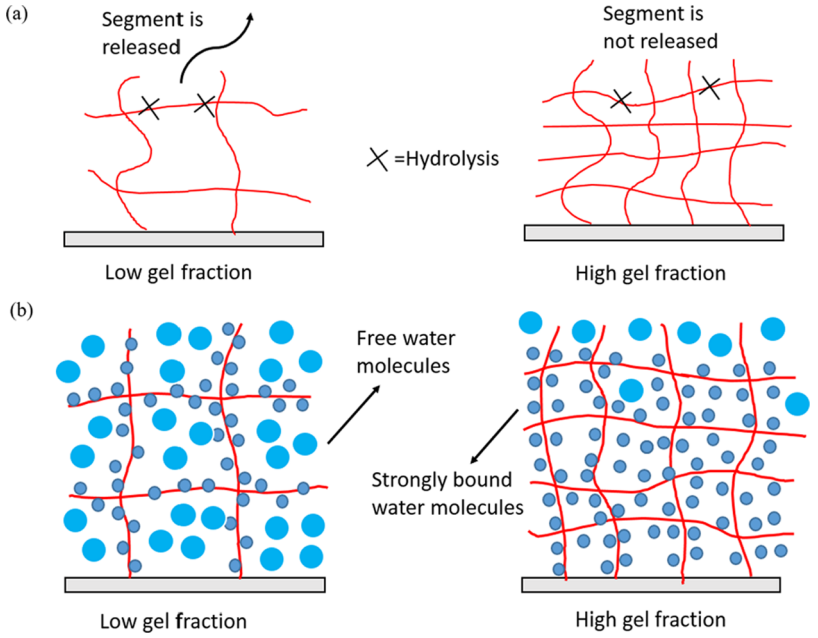

Figure 4. Degradation of the crosslinked network thin film in PBS buffer solution via hydrolysis of ester is controlled by the probability of releasing segments (a) or mobility of water molecules in the networks (b).

higher probability of releasing a segment for a given number of cleaved ester bonds in a low gel fraction network. This is illustrated in the cartoon in Figure 4a. Conversely, in a higher gel fraction network with a higher crosslink density, there is a lower probability of releasing a segment for the same number of cleaved ester bonds (Figure 4b). The second explanation is, when the gel fraction is low, water molecules can penetrate the network more efficiently, hydrolyze the network more extensively, and carry the degraded segments out. However, if the gel fraction is high, the mobility of water molecules will be restricted. Therefore, the hydrolysis is limited mainly to the water/film interface. This latter explanation is consistent with the observations that the degradation of high gel fraction networks is independent of thickness (zeroth-order kinetics). In contrast, the degradation of low gel fraction networks depends on the thickness (first-order kinetics).

To verify that the degradation of the networks was not caused by the main-chain scission induced by osmotic pressure due to solvent swelling,[24] thin films with different gel fractions were immersed in dry DCM. DCM was chosen because it does not induce hydrolysis of ester linkages and swells the polyester gel very well (with a swelling ratio of 5.20). After 24 h, the thicknesses of all films did not change, suggesting that this mechanism for main-chain scission is not operative here.

Protein Adsorption. Protein adsorption behaviors of these films were studied in stock solution with different protein concentrations and ionic strengths. We found that the BSA adsorption is slower in higher ionic strength PBS solution. There are two explanations. First, to adsorb on surfaces, BSA needs to expose, at least partially, its hydrophobic core to surfaces by changing its conformation. However, the increasing salt concentration will stabilize the native BSA conformation through interaction between phosphate and BSA, and this effect decreases the adsorption efficiency.[25] Moreover, ions can also destabilize the hydrophobic interaction between protein and the polymer film.[26] The first set of conditions employed a 1 mg/mL albumin−fluorescein isothiocyanate conjugate protein in phosphate-buffered saline (PBS) with a pH of 7.4 and a total ionic strength of 1 M. In this case, the amount of protein adsorbed on surfaces is too small to observe a change in film thickness. Thus, the samples were taken out of the protein solution at various times and observed under a

https://doi.org/10.1021/acs.langmuir.1c00890
Langmuir 2021, 37, 8978−8988

fluorescence microscope. The adsorbed protein was estimated to be proportional to the measured fluorescence intensity. The images in Figure S32 are collected by fluorescence microscope after immersing 2.5, 3.5, 4.3, 5, 7.5, and 10% EBP feed ratio networks in FITC−BSA stock solution for 47.5 h at room temperature.

By integrating the fluorescence intensity of each image, intensity versus time plots were constructed (Figure 5). The

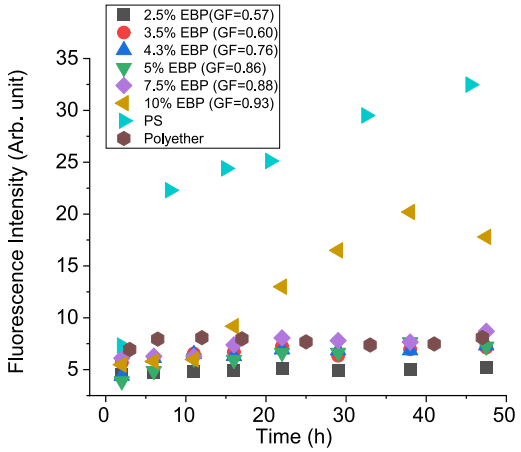

Figure 5. Plot showing fluorescence intensity of thin films with different gel fractions immersed in a stock solution with pH 7.4, ionic strength 1 M, 1 mg/mL fluorescently labeled BSA at specific immersion times.

fluorescence intensity reflects the relative amount of FITC−BSA adsorbed. The networks with low gel fraction resisted protein adsorption compared with a polystyrene and polyether (Figure S9) reference (Figure 5). The latter has a similar structure to the polyesters but has a nondegradable ether backbone. It permits a reasonable comparison of the protein resistance between chemically similar, static, and dynamic surfaces. The results indicate that the amount of FITC−BSA adsorbed on polyester networks is lower than on polystyrene, and smaller amount of FITC−BSA adsorbed on low gel fraction networks compared with static polyether film for a long period of time. However, relatively more FITC−BSA adsorption was observed on high gel fraction networks. Three reasons might explain this behavior. First, protein adsorption is driven by the hydrophobic interactions between proteins and surfaces. As EBP is hydrophobic, networks with more EBP expose more hydrophobic segments to protein, making protein adsorption favorable. Second, the more lightly crosslinked networks are more extensively hydrated (see below), and a hydrated network is more hydrophilic and less prone to protein adsorption. Third, the degradation of the network with a high gel fraction is slower than that of networks with a lower gel fraction. The degradation rate of higher gel fraction networks might be slower than the rate of protein adsorption, so degradation may have less of a role in shedding (e.g., sloughing off) any adsorbed protein, in which case protein accumulates on the surface.

The second set of conditions employed a 3 mg/mL BSA solution in phosphate-buffered saline (PBS) with a pH of 7.4 and a total ionic strength of 100 mM. The protein is more likely to adsorb on the surface under these conditions due to the higher concentration and lower ionic strength. For each gel fraction, we prepared two networks. One was incubated in PBS solution, and another was incubated in the BSA stock solution for comparison. The two wafers were agitated under identical conditions and for the same duration. Both specimens were removed at the same time, and their thicknesses were measured. In Figure 6, the red lines indicate the thickness of the film in the BSA stock solution at various total immersion times, and the black lines indicate the thickness of the film in

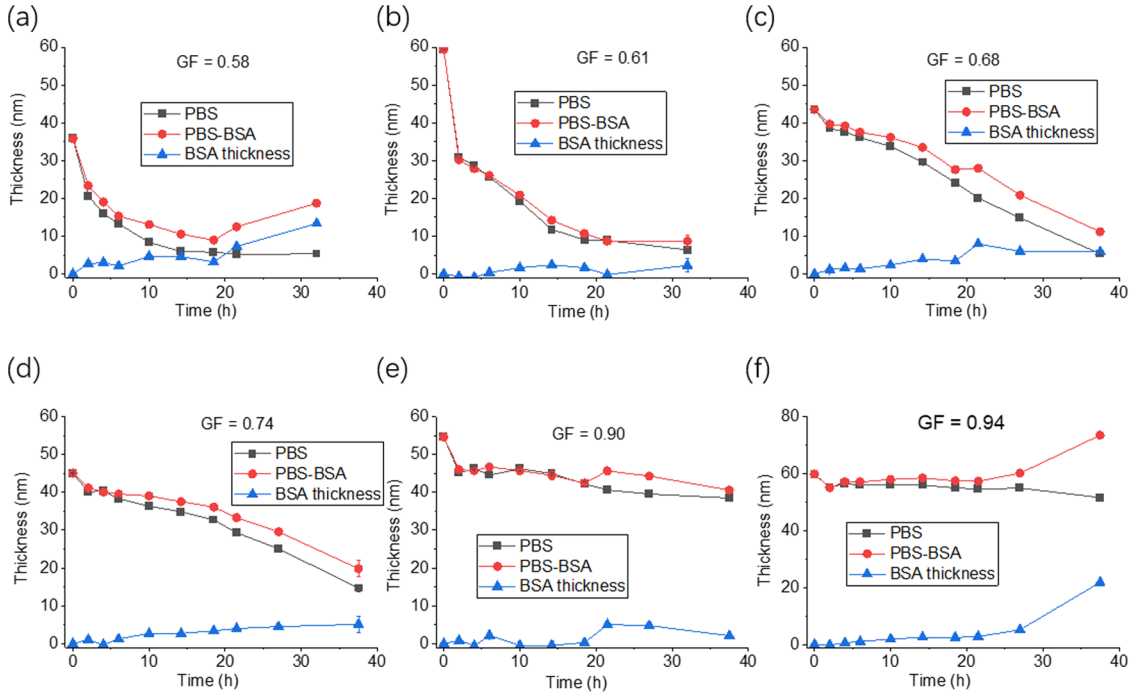

Figure 6. Plots showing the thickness of thin films with various gel fractions immersed in BSA−PBS solution (ionic strength 100 mM, pH 7.4, BSA 3 mg/mL) for various times. Thicknesses were obtained via ellipsometry.

https://doi.org/10.1021/acs.langmuir.1c00890
Langmuir 2021, 37, 8978−8988

PBS solution. The blue line, obtained by subtracting the black line from the red line, represents the net, adsorbed BSA thickness. This analysis does, admittedly, assume that the film degradation is identical under the two conditions. Error bars within a given sample are small, as stated in the caption to Figure 6. However, we acknowledge that there likely is variability from sample to sample. However, preparing multiple samples with identical thicknesses and gel fractions is difficult or impossible. The variability of the gel fraction of the samples in each plot is in the range of ±1 to ±5%. Within this uncertainty, however, the stated conclusions are still valid. In Figure 6a, the BSA starts to adsorb on the surface after complete film degradation. In Figure 6b−e, there is little protein adsorbed on the surfaces. Thus, these films resist protein adsorption for their entire lifetimes. In Figure 6f, the BSA starts to adsorb on the surface after 27 h immersion, arising from the high gel fraction of the network. The effect of gel fraction on antifouling capability of the network was discussed previously. Although error bars are very small for each experiment, the calculation of protein thickness ignores the effect of transiently adsorbed protein on the degradation of the networks, which may contribute to uncertainty in values.

PS and polyether (Figure S9) coatings were prepared and immersed in BSA stock solutions for comparison. Figure 7 illustrates that the PS coating resisted significant protein adsorption for ca. 18 h. The static polyether coating resisted protein adsorption for ca. 28 h and dynamic polyester coatings resisted protein adsorption for ca. 38 h. Therefore, dynamic polyester surfaces have better protein resistance under these conditions. It is observed that there is always 2 nm protein adsorbed on all surfaces after immersion in the BSA solution. This phenomenon for BSA was also reported in the literature.[8,11] It is possible that BSA is reversibly attached to surfaces in a dynamic equilibrium.

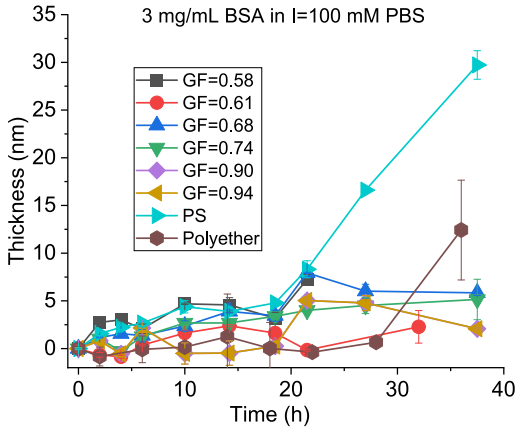

Figure 7. Plots showing calculated BSA thickness on polyester, PS, and polyether thin films. Each data point is the average value of three measurements on different locations of the film. Some error bars are smaller than the size of the plot symbols used.

Characterization of Film Hydration and Surface Hydrophilicity. Although the adsorption of proteins could have been inhibited by the degradation of the networks and sloughing off of any initially adsorbed protein, there is evidence that the relative hydration and thus hydrophilicity of the networks may play a role. Thus, the swelling behavior and water contact angles of the films were investigated. These are two complementary ways to judge the hydration and hydrophilicity of the films.

Swelling Behavior. The swollen thickness of the thin films was measured by VASE following a literature procedure.[11] After measuring the thickness of the dry film, an ellipsometry cell was filled with ∼100 mL of DI water, the sample was immersed and left for 1 min to reach equilibrium, and then the thickness of the film in water was measured and marked as d_{wet}. The swelling ratio of the film (α) was calculated using eqs 7 and 8.

$$\alpha = \frac{d_{wet}}{d_{dry}} \tag{7}$$

The solvent fraction (φ) describing the water content in the network was calculated as

$$\varphi = 1 - \frac{1}{\alpha} \tag{8}$$

Figure 8a plots the swelling ratio of polyesters as a function of gel fraction. For comparison, the swelling ratios of synthesized polyether with 5% crosslinker and polystyrene are 2.47 ± 0.14 and 0.97 ± 0.07, respectively. The degree of swelling is influenced strongly by the gel fraction of the networks. The networks with low gel fraction exhibit a large degree of swelling. With the increase of the gel fraction, the degree of swelling decreases. The swelling behavior correlates with the hypothesis given previously for the degradation kinetics. At a low gel fraction, water can penetrate the network

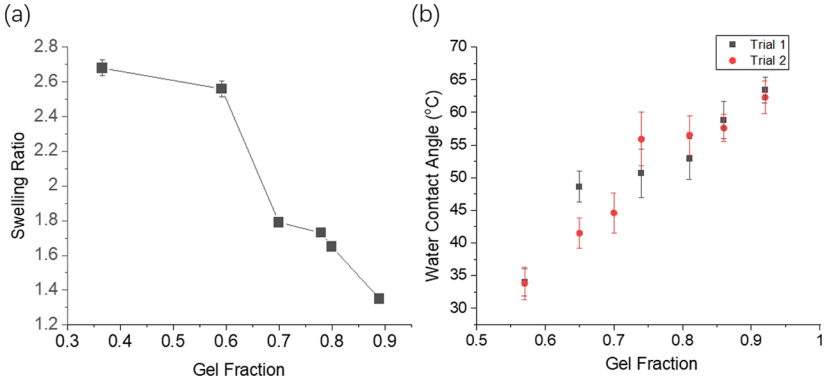

Figure 8. (a) Plot of the swelling ratios of networks with different gel fractions in DI water. (b) Plot showing water contact angle of polymer thin films with different gel fractions. Some error bars are smaller than the size of the plot symbols used.

https://doi.org/10.1021/acs.langmuir.1c00890
Langmuir 2021, 37, 8978−8988

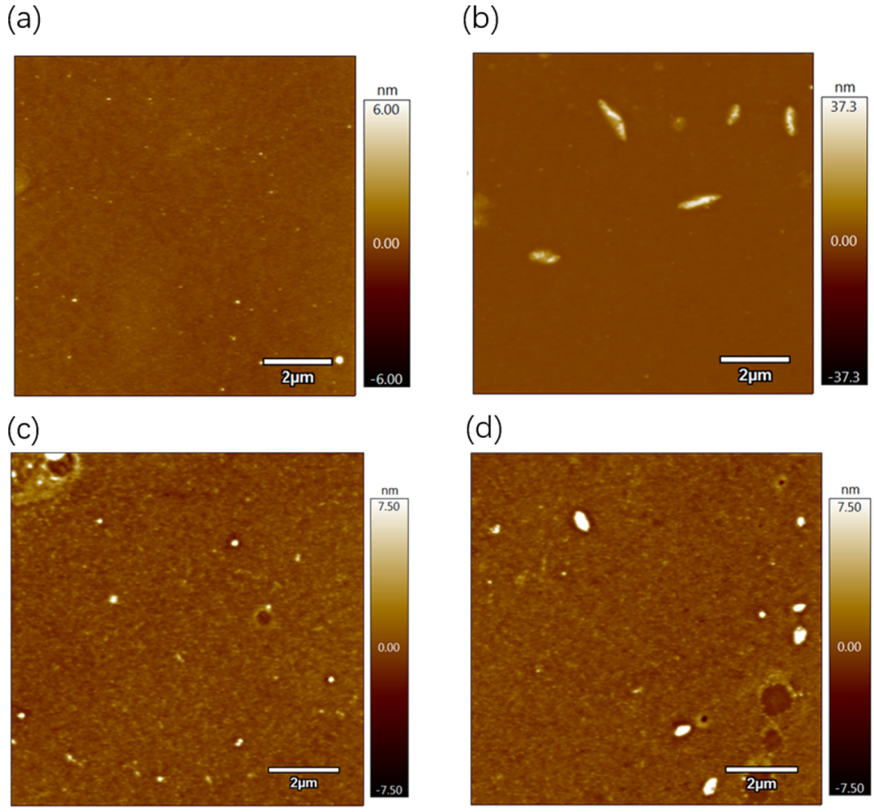

Figure 9. AFM images showing the surface morphology of 7.5% EBP polyester after immersing in 3 mg/mL BSA, pH = 7.4, ionic strength = 100 mM PBS buffer solution after (a) 0 h, (b) 2 h, (c) 10 h, and (d) 24 h.

freely and network chains are more flexible. At a higher gel fraction, the mobility of water molecules is restricted and network chains are less flexible, so the swelling ratio and solvent fraction are lower. Moreover, the swelling ratio at a low gel fraction might also be affected by imperfect networks. The network may swell to a different extent in different locations on samples with a low gel fraction. We used average thickness measured by VASE to calculate the swelling ratio.

These data are consistent with a highly hydrated film being more resistant to protein adsorption. Genzer et al. determined that the amount of fibrinogen (Fg) adsorbed on hydrogel substrates depends on the degree of crosslinking and the swelling capacity of networks.[11] This previous work was focused on resisting fibrinogen adsorption by poly(N-isopropylacrylamide) hydrogels in contrast to the work here, which focuses on BSA resistance by the novel polyester networks. Nevertheless, there are behaviors that are profitably compared. They concluded that, for hydrophilic coatings, the enthalpy contribution to the protein adsorption process could be ignored. Therefore, the Gibbs free energy of adsorption was dominated by entropy change during the process. Although entropy increases when proteins penetrate the networks, it does not compensate for entropy loss due to reduced freedom of swollen chains. Such entropically driven resistance was termed "entropic shielding." The higher swelling ratio of lower gel fraction networks indicates a higher degree of freedom, in which the system needs to sacrifice more entropy for the adsorption of proteins. Therefore, the protein adsorption on highly swollen networks is entropically unfavorable.[11]

Contact Angle Measurements. To judge the relative hydrophilicity of coatings, they were characterized by water contact angle measurements. A graph showing how the contact angle varied with gel fraction is given in Figure 8b. For comparison, the water contact angles of spin-coated polyether with 5% crosslinker and polystyrene surfaces are 49 ± 4.7 and 90 ± 0.5°, respectively. We recognize that contact angles, as defined by the Young's equation, are measured on impenetrable surfaces. Still, within the samples, the water contact angle varied substantially (ca. 30°) in our systems. This phenomenon is not surprising since EBP units were expected to impede the hydrophilicity of the overall polymer. Moreover, the higher degree of crosslinking afforded by films with a greater percentage of EBP units reduced the degree of hydration of the films, also rendering them less hydrophilic. It is reasonable to imagine that hydrophilicity differences play a role in the relative affinity of proteins to adsorb to the various films.

Characterization by AFM. To probe the onset of protein adsorption and morphology of the surface, atomic force microscopy (AFM) was performed. A set of samples synthesized with 7.5% EBP feed ratio was prepared and crosslinked. These specimens were immersed in a 3 mg/mL BSA stock solution for 2, 10, and 24 h. These samples were chosen to give a reasonably long time window before the complete degradation of the film occurred. Representative AFM images are shown in Figure 9. The bright areas are interpreted as BSA islands and dark areas as regions of pitting. Figure 9a shows the AFM image of the film before incubation in BSA solution. The RMS value of the surface is 0.18 nm (Figure S33), indicating that the surface was relatively uniform. For comparison, the RMS roughness of the polyether sample was 0.35 nm (Figure S34) and the RMS roughness of the polystyrene sample was 0.72 nm (Figure S35). In Figure 9b, some accumulation of BSA is visible at 2 h. The height of these

https://doi.org/10.1021/acs.langmuir.1c00890
Langmuir 2021, 37, 8978−8988

islands is greater than that expected for a monolayer of BSA (monomeric BSA has dimensions of 4 × 4 × 14 nm^3).[27] This indicates that BSA forms islands on the films suggesting that BSA has a greater affinity to adhere to itself than to the films. At 10 h (Figure 9c) and 24 h (Figure 9d) time points, one can note an increase in the background roughness of the film and some pitting. These features are consistent with the hydrolytic degradation of the films. There is less protein accumulation observable compared to the sample prepared with a 2 h incubation time in BSA solution, indicating desorption of BSA.

CONCLUSIONS

We prepared surface-attached degradable polyester networks and investigated their degradation, protein resistance, hydrophilicity, and swellability. The crosslink density was tuned by altering the mole fraction of EBP in the polymer (from 2.5 to 10%). Networks with lower EBP mole fractions had lower gel fractions, higher swelling ratios, and faster degradation, which followed first-order degradation kinetics. Conversely, networks with higher EBP mole fraction had higher gel fractions, lower swelling ratios, and slower degradation, and their degradation followed zeroth-order kinetics. The network degradation was accelerated under basic or acidic conditions, consistent with previously observed rates of ester hydrolysis. The adsorption of BSA on surface-attached polyester networks was also studied under different concentrations and ionic strength. The results showed that the novel dynamic surfaces resisted BSA adsorption better than PS or static, polyether-based surfaces with a similar chemical structure. The networks with lower crosslink densities resist BSA better through entropic shielding and faster degradation, while densely crosslinked networks exhibit more BSA adsorption due to increased hydrophobic−hydrophobic interaction between networks and BSA and slower degradation. This work sets a precedent for resisting protein adsorption via eco-friendly, dynamic surfaces, and we believe that these dynamic surfaces could be highly impactful for the field of biomedical implants, biosensors, and drug carriers in the future.

ASSOCIATED CONTENT

Supporting Information

The Supporting Information is available free of charge at https://pubs.acs.org/doi/10.1021/acs.langmuir.1c00890.

Schemes for the synthesis of molecules and polymers prepared; ^1H and ^{13}C NMR data of molecules and polymers prepared; and supporting data for polymerization, crosslinking, degradation, and protein adsorption (PDF)

AUTHOR INFORMATION

Corresponding Author

Christopher B. Gorman − *Department of Chemistry, North Carolina State University, Raleigh, North Carolina 27695-7905, United States;* orcid.org/0000-0001-7367-2965; Email: cbgorman@ncsu.edu

Authors

Gaoyan Mu − *Department of Chemistry, North Carolina State University, Raleigh, North Carolina 27695-7905, United States*

C. K. Pandiyarajan − *Department of Chemical & Biomolecular Engineering, North Carolina State University, Raleigh, North Carolina 27695-7905, United States;* orcid.org/0000-0002-8954-9141

Xiuyuan Lu − *Department of Chemistry, North Carolina State University, Raleigh, North Carolina 27695-7905, United States*

Matt Weaver − *Department of Chemistry, North Carolina State University, Raleigh, North Carolina 27695-7905, United States*

Jan Genzer − *Department of Chemical & Biomolecular Engineering, North Carolina State University, Raleigh, North Carolina 27695-7905, United States;* orcid.org/0000-0002-1633-238X

Complete contact information is available at: https://pubs.acs.org/10.1021/acs.langmuir.1c00890

Notes

The authors declare no competing financial interest.

ACKNOWLEDGMENTS

The authors thank Professor Geoffrey Coates (Cornell) for helpful discussions. C.K.P. was supported by the S. Frank and Doris Culberson funds awarded to J.G. In addition, the authors appreciate partial support from a grant DMR-1809453 awarded to J.G. This work was performed in part by the Molecular Education, Technology and Research Innovation Center (METRIC) at NC State University, which is supported by the State of North Carolina. Part of this work was also performed in part at the Analytical Instrumentation Facility (AIF) at North Carolina State University, which is supported by the State of North Carolina and the National Science Foundation (Award Number ECCS-2025064). The AIF is a member of the North Carolina Research Triangle Nanotechnology Network (RTNN), a site in the National Nanotechnology Coordinated Infrastructure (NNCI).

REFERENCES

(1) Abbott, A.; Abel, P. D.; Arnold, D. W.; Milne, A. Cost−benefit analysis of the use of TBT: the case for a treatment approach. *Sci. Total Environ.* **2000**, *258*, 5−19.

(2) Magill, S. S.; Edwards, J. R.; Bamberg, W.; Beldavs, Z. G.; Dumyati, G.; Kainer, M. A.; Lynfield, R.; Maloney, M.; McAllister-Hollod, L.; Nadle, J.; Ray, S. M.; Thompson, D. L.; Wilson, L. E.; Fridkin, S. K. Multistate point-prevalence survey of health care-associated infections. *N. Engl. J. Med.* **2014**, *370*, 1198−1208.

(3) Bixler, G. D.; Bhushan, B. Biofouling: lessons from nature. *Philos. Trans. R. Soc., A* **2012**, *370*, 2381−2417.

(4) Kousar, F.; Malmström, J.; Swift, S.; Ross, J.; Perera, J.; Moratti, S. C. Protein-Resistant Behavior of Poly(ethylene glycol)-Containing Polymers with Phosphonate/Phosphate Units on Stainless Steel Surfaces. *ACS Appl. Polym. Mater.* **2021**, *3*, 2785−2801.

(5) (a) Hu, P.; Xie, Q.; Ma, C.; Zhang, G. Silicone-Based Fouling-Release Coatings for Marine Antifouling. *Langmuir* **2020**, *36*, 2170−2183. (b) Xu, B.; Liu, Y.; Sun, X.; Hu, J.; Shi, P.; Huang, X. Semifluorinated Synergistic Nonfouling/Fouling-Release Surface. *ACS Appl. Mater. Interfaces* **2017**, *9*, 16517−16523. (c) Sun, X.; Wu, C.; Hu, J.; Huang, X.; Lu, G.; Feng, C. Antifouling Surfaces Based on Fluorine-Containing Asymmetric Polymer Brushes: Effect of Chain Length of Fluorinated Side Chain. *Langmuir* **2019**, *35*, 1235−1241.

(6) (a) Lin, X.; Jain, P.; Wu, K.; Hong, D.; Hung, H.-C.; O'Kelly, M. B.; Li, B.; Zhang, P.; Yuan, Z.; Jiang, S. Ultralow Fouling and Functionalizable Surface Chemistry Based on Zwitterionic Carboxybetaine Random Copolymers. *Langmuir* **2019**, *35*, 1544−1551. (b) Brown, M. U.; Triozzi, A.; Emrick, T. Polymer Zwitterions with Phosphonium Cations. *J. Am. Chem. Soc.* **2021**, *143*, 6528−6532.

(7) Guo, H.; Chen, P.; Tian, S.; Ma, Y.; Li, Q.; Wen, C.; Yang, J.; Zhang, L. Amphiphilic Marine Antifouling Coatings Based on a Hydrophilic Polyvinylpyrrolidone and Hydrophobic Fluorine−Silicon-Containing Block Copolymer. *Langmuir* **2020**, *36*, 14573−14581.
(8) Hu, X.; Gorman, C. B. Resisting protein adsorption on biodegradable polyester brushes. *Acta Biomater.* **2014**, *10*, 3497−3504.
(9) Xu, B.; Feng, C.; Lv, Y.; Lin, S.; Lu, G.; Huang, X. Biomimetic Asymmetric Polymer Brush Coatings Bearing Fencelike Conformation Exhibit Superior Protection and Antifouling Performance. *ACS Appl. Mater. Interfaces* **2020**, *12*, 1588−1596.
(10) (a) Xu, B.; Feng, C.; Hu, J.; Shi, P.; Gu, G.; Wang, L.; Huang, X. Spin-Casting Polymer Brush Films for Stimuli-Responsive and Anti-Fouling Surfaces. *ACS Appl. Mater. Interfaces* **2016**, *8*, 6685−6692. (b) Feng, C.; Huang, X. Polymer Brushes: Efficient Synthesis and Applications. *Acc. Chem. Res.* **2018**, *51*, 2314−2323.
(11) Pandiyarajan, C. K.; Genzer, J. Effect of Network Density in Surface-Anchored Poly(N-isopropylacrylamide) Hydrogels on Adsorption of Fibrinogen. *Langmuir* **2017**, *33*, 1974−1983.
(12) (a) Blond, P.; Bevernaegie, R.; Troian-Gautier, L.; Lagrost, C.; Hubert, J.; Reniers, F.; Raussens, V.; Jabin, I. Ready-to-Use Germanium Surfaces for the Development of FTIR-Based Biosensors for Proteins. *Langmuir* **2020**, *36*, 12068−12076. (b) Zarski, P.; Ryder, A. G. Super Stable Fluorescein Isothiocyanate Isomer I Monolayer for Total Internal Reflection Fluorescence Microscopy. *Langmuir* **2018**, *34*, 10913−10923. (c) Schneider, C. A.; Rasband, W. S.; Eliceiri, K. W. NIH Image to ImageJ: 25 years of image analysis. *Nat. Methods* **2012**, *9*, 671−675.
(13) Kankate, L.; Werner, U.; Turchanin, A.; Gölzhäuser, A.; Grossmann, H.; Tampé, R. Protein resistant oligo(ethylene glycol) terminated self-assembled monolayers of thiols on gold by vapor deposition in vacuum. *Biointerphases* **2010**, *5*, 30−36.
(14) (a) Li, S.; Guo, Z.; Zhang, H.; Li, X.; Li, W.; Liu, P.; Ren, Y.; Li, X. ABC Triblock Copolymers Antibacterial Materials Consisting of Fluoropolymer and Polyethylene Glycol Antifouling Block and Quaternary Ammonium Salt Sterilization Block. *ACS Appl. Bio Mater.* **2021**, *4*, 3166−3177. (b) Shuai, C.-X.; He, Y.; Su, P.; Huang, Q.; Pan, D.; Xu, Q.; Feng, D.; Jiang, Y. Integration of PEGylated Polyaniline Nanocoatings with Multiple Plastic Substrates Generates Comparable Antifouling Performance. *Langmuir* **2020**, *36*, 9114−9123.
(15) (a) DiCiccio, A. M.; Coates, G. W. Ring-Opening Copolymerization of Maleic Anhydride with Epoxides: A Chain-Growth Approach to Unsaturated Polyesters. *J. Am. Chem. Soc.* **2011**, *133*, 10724−10727. (b) DiCiccio, A. M.; Longo, J. M.; Rodríguez-Calero, G. G.; Coates, G. W. Development of Highly Active and Regioselective Catalysts for the Copolymerization of Epoxides with Cyclic Anhydrides: An Unanticipated Effect of Electronic Variation. *J. Am. Chem. Soc.* **2016**, *138*, 7107−7113.
(16) (a) Longo, J. M.; Sanford, M. J.; Coates, G. W. Ring-Opening Copolymerization of Epoxides and Cyclic Anhydrides with Discrete Metal Complexes: Structure−Property Relationships. *Chem. Rev.* **2016**, *116*, 15167−15197. (b) Huijser, S.; HosseiniNejad, E.; Sablong, R.; de Jong, C.; Koning, C. E.; Duchateau, R. Ring-Opening Co- and Terpolymerization of an Alicyclic Oxirane with Carboxylic Acid Anhydrides and CO_2 in the Presence of Chromium Porphyrinato and Salen Catalysts. *Macromolecules* **2011**, *44*, 1132−1139. (c) Winkler, M.; Romain, C.; Meier, M. A. R.; Williams, C. K. Renewable polycarbonates and polyesters from 1,4-cyclohexadiene. *Green Chem.* **2015**, *17*, 300−306. (d) Liu, Y.; Guo, J.-Z.; Lu, H.-W.; Wang, H.-B.; Lu, X.-B. Making Various Degradable Polymers from Epoxides Using a Versatile Dinuclear Chromium Catalyst. *Macromolecules* **2018**, *51*, 771−778.
(17) (a) Hu, L.-F.; Zhang, C.-J.; Chen, D.-J.; Cao, X.-H.; Yang, J.-L.; Zhang, X.-H. Synthesis of High-Molecular-Weight Maleic Anhydride-Based Polyesters with Enhanced Properties. *ACS Appl. Polym. Mater.* **2020**, *2*, 5817−5823. (b) Ye, S.; Wang, W.; Liang, J.; Wang, S.; Xiao, M.; Meng, Y. Metal-Free Approach for a One-Pot Construction of Biodegradable Block Copolymers from Epoxides, Phthalic Anhydride, and CO2. *ACS Sustainable Chem. Eng.* **2020**, *8*, 17860−17867. (c) Chen, C.-M.; Xu, X.; Ji, H.-Y.; Wang, B.; Pan, L.; Luo, Y.; Li, Y.-S. Alkali Metal Carboxylates: Simple and Versatile Initiators for Ring-Opening Alternating Copolymerization of Cyclic Anhydrides/Epoxides. *Macromolecules* **2021**, *54*, 713−724.
(18) (a) Wu, Q.; Qu, B. Photoinitiating characteristics of benzophenone derivatives as new initiators in the photocrosslinking of polyethylene. *Polym. Eng. Sci.* **2001**, *41*, 1220−1226. (b) Yu, L.; Hou, Y.; Cheng, C.; Schlaich, C.; Noeske, P.-L. M.; Wei, Q.; Haag, R. High-Antifouling Polymer Brush Coatings on Nonpolar Surfaces via Adsorption-Cross-Linking Strategy. *ACS Appl. Mater. Interfaces* **2017**, *9*, 44281−44292.
(19) Carroll, G. T.; Sojka, M. E.; Lei, X.; Turro, N. J.; Koberstein, J. T. Photoactive Additives for Cross-Linking Polymer Films: Inhibition of Dewetting in Thin Polymer Films. *Langmuir* **2006**, *22*, 7748−7754.
(20) Hu, X.; Hu, G.; Crawford, K.; Gorman, C. B. Comparison of the growth and degradation of poly(glycolic acid) and poly(ε-caprolactone) brushes. *J. Polym. Sci., Part A: Polym. Chem.* **2013**, *51*, 4643−4649.
(21) (a) Zheng, N.; Xu, Y.; Zhao, Q.; Xie, T. Dynamic Covalent Polymer Networks: A Molecular Platform for Designing Functions beyond Chemical Recycling and Self-Healing. *Chem. Rev.* **2021**, *121*, 1716−1745. (b) Muroya, T.; Yamamoto, K.; Aoyagi, T. Degradation of cross-linked aliphatic polyester composed of poly(ε-caprolactone-co-d,l-lactide) depending on the thermal properties. *Polym. Degrad. Stab.* **2009**, *94*, 285−290. (c) Amsden, B. G.; Tse, M. Y.; Turner, N. D.; Knight, D. K.; Pang, S. C. In Vivo Degradation Behavior of Photo-Cross-Linked star-Poly(ε-caprolactone-co-d,l-lactide) Elastomers. *Biomacromolecules* **2006**, *7*, 365−372. (d) Gu, X.; Raghavan, D.; Nguyen, T.; VanLandingham, M. R.; Yebassa, D. Characterization of polyester degradation using tapping mode atomic force microscopy: exposure to alkaline solution at room temperature. *Polym. Degrad. Stab.* **2001**, *74*, 139−149.
(22) Abeysinghe, H. P.; Edwards, W.; Pritchard, G.; Swampillai, G. J. Degradation of crosslinked resins in water and electrolyte solutions. *Polymer* **1982**, *23*, 1785−1790.
(23) Jung, J. H.; Ree, M.; Kim, H. Acid- and base-catalyzed hydrolyses of aliphatic polycarbonates and polyesters. *Catal. Today* **2006**, *115*, 283−287.
(24) Messmer, D.; Bertran, O.; Kissner, R.; Alemán, C.; Schlüter, A. D. Main-chain scission of individual macromolecules induced by solvent swelling. *Chem. Sci.* **2019**, *10*, 6125−6139.
(25) Jeyachandran, Y. L.; Mielczarski, E.; Rai, B.; Mielczarski, J. A. Quantitative and Qualitative Evaluation of Adsorption/Desorption of Bovine Serum Albumin on Hydrophilic and Hydrophobic Surfaces. *Langmuir* **2009**, *25*, 11614−11620.
(26) Luey, J.-K.; McGuire, J.; Sproull, R. D. The effect of pH and NaCl concentration on adsorption of β-lactoglobulin at hydrophilic and hydrophobic silicon surfaces. *J. Colloid Interface Sci.* **1991**, *143*, 489−500.
(27) Wright, A. K.; Thompson, M. R. Hydrodynamic structure of bovine serum albumin determined by transient electric birefringence. *Biophys. J.* **1975**, *15*, 137−141.

https://doi.org/10.1021/acs.langmuir.1c00890
Langmuir 2021, 37, 8978−8988